Neurocomputing 496 (2022) 147–157

Contents lists available at ScienceDirect

Neurocomputing

journal homepage: www.elsevier.com/locate/neucom

Model design for networks of heterogeneous Hodgkin–Huxley neurons

A.G. Giannari [a,*], A. Astolfi [a,b]

[a] Department of Electrical and Electronic Engineering, Imperial College London, London SW7 2AZ, UK
[b] Dipartimento di Ingegneria Civile e Ingegneria Informatica, Università di Roma "Tor Vergata", Via del Politecnico, 100133 Roma, Italy

ARTICLE INFO

Article history:
Received 10 January 2022
Revised 25 March 2022
Accepted 23 April 2022
Available online 27 April 2022

Keywords:
Hodgkin–Huxley model
Neuronal networks
Heterogeneous firing patterns
Synaptic coupling
Graph theory
Feedback

ABSTRACT

We present a novel modular, scalable and adaptable modelling framework to accurately model neuronal networks composed of neurons with different dynamic properties and distinct firing patterns based on a control-inspired feedback structure. We consider three important classes of neurons: inhibitory Fast spiking neurons, excitatory regular spiking with adaptations neurons, and excitatory intrinsic bursting neurons. We also take into consideration two basic means of neuronal interconnection: electrical and chemical synapses. By separating the neuronal dynamics from the network dynamics, we have developed a fully flexible feedback structure that can be further augmented to incorporate additional types of neurons and/or synapses. We use an augmented version of the Hodgkin–Huxley model to describe the individual neuron dynamics and graph theory to define the network structure. We provide simulation results for small fundamental neuron motifs as well as bigger neuronal networks and we verify the accuracy, flexibility and scalability of the proposed method. Therefore, we provide the basis for a comprehensive modelling framework that is able to imitate the dynamics of individual neurons and neuronal networks and is able to replicate basic normal brain function. The structure of the proposed framework is ideal for applications of control and optimization methods both for modelling the effect of pharmacological substances as well as for modelling diseased neuron and network conditions.

1. Introduction

In 1952 Hodgkin and Huxley published the first quantitative model that describes the creation and propagation of action potentials in neurons by conducting in vivo patch clamp experiments on a nerve axon of a giant squid [1]. Following this breakthrough the Hodgkin and Huxley (HH) model has been extensively used to understand the complexity of neurons [2–5] and neuronal networks [6–9] and it is effectively considered to be the most accurate and efficient model that describes neuronal behavior [10]. In addition the HH model, despite being computationally expensive, is considered to be the most reliable and bio-physically meaningful model among the existing models, such as the Integrate and Fire, the FitzHugh-Nagumo, the Hindmarsh-Rose and the Izhikevich models as discussed in [11].

The HH model exclusively describes the dynamics of a single giant squid neuron. For this reason, attempts have been made to take into consideration the biophysical and dynamical characteristics of mammalian neurons, by altering the original HH model. The modified HH model in [12] accurately predicts spiking sequences of biological neurons under the influence of fluctuating input currents while the augmented version of the HH model in [13] mimics the properties of oscillations in bursting, a typical firing pattern observed in mammals. Finally, in [14], experimental results from 4 types of neurons have been fitted to modified HH models able to reproduce their distinct firing patterns.

The study of neuronal dynamics, however insightful for the function of mammalian brain cells, is not sufficient to describe the complex functions executed by the interconnections of neurons through which information propagates. For this reason, efforts have been concentrated on the study of the collective dynamics of neuronal networks rather than on the ones of an individual neuron. In addition, graph theory has been immersed in the field of neuroscience in an effort to understand the dynamics of brain networks and their functionality, see e.g. [15–17]. The modelling of the network topology can be achieved using directed graphs, in which the nodes represent the individual neurons and the edges correspond to their coupling [18].

The modelling of large-scale neuronal networks requires the manipulation of highly nonlinear coupled differential equations. The complexity and large dimensionality of a Hodgkin–Huxley-based network model, that can provide an explicit and realistic representation of the brain function, renders its analysis complex and its use in the scientific community scarce. Despite the existence and

* Corresponding author.
E-mail addresses: ag3614@ic.ac.uk (A.G. Giannari), a.astolfi@imperial.ac.uk (A. Astolfi).

https://doi.org/10.1016/j.neucom.2022.04.115
0925-2312/

continuing development of numerous software platforms (e.g. Neuron [19], Neuroconstruct [20], Brian [21]) that are purposed for simulating neuronal networks, there is lack of a unified and compact modelling framework to act as a basis for future simulators. Our aim is not to replace already existing powerful software but to provide an advanced universal modelling method that is independent of the simulator environment. Besides, the existence of distinct modelling techniques is important for their validation and therefore the growth of the field of neuroscience [22].

In this paper, we introduce a novel, scalable, adaptable and modular modelling framework that is based on a control-inspired feedback structure and accurately models neuronal networks with different firing patterns, dynamic properties and coupling mechanisms. Scalability refers to the ability of the model to handle an increased number of neurons and therefore state variables and parameters. Adaptability refers to the ability of the model to be augmented with more equations or change on-demand either on a neuron or network level, e.g. parameters, connectivity. Modularity, in this context, refers to the ability of the model to separate the dynamics of heterogeneous neurons in modules that are able to communicate with each other. Model modularity enables the generation of large-scale networks from sub-modules that can be tested and validated separately before studying their effect on the large network and is inherently related to the flexibility of the model by allowing incrementing changes [23]. For the purpose of creating a network model with all the above characteristics, we have merged the modified HH equations for three distinct neuronal firing patterns commonly observed in the human brain, see [14] (with some parameter adaptations). We have also incorporated equations for two distinct types of synaptic coupling: electrical and chemical. Moreover, we have used graph theory to create a feedback structure that separates the model and network dynamics and it is therefore straightforward for in silico implementation. Finally, to verify the accuracy and the scalability of the proposed modelling framework we have modeled and validated multiple neuron motifs that are responsible for important functions as well as a larger random network. The validity of the HH network model is supported by the combination of experimentally derived parameters for the neuron dynamics and tuned connectivity parameters subject to constraints to match the target functionality of the simulated neuronal motifs.

The proposed HH network model is an augmented version of the original HH model that is able to describe the behaviour of large-scale heterogeneous and biologically realistic networks of neurons with meaningful parameters.

One of the biggest advantages of the feedback structure is the separation of the neuron and network dynamics which reduces the complexity of the overall system while allowing the independent manipulation of the neuron and network parameters. The separation facilitates the compact description of the network dynamics via the direct control of the connectivity matrices without compromising the interaction of individual neurons with the network. The dynamics of the individual neurons are governed by the injected current, the network structure and their physiological characteristics. Assuming that the physiological characteristics of the neurons remain the same, the process of defining a unique brain activity is reduced to choosing the desired neuronal types involved, the appropriate external input current, and the two connectivity matrices that correspond to the electrical and chemical connections associated with the desired network. Therefore, the proposed feedback structure is ideal for parameter optimization and control applications both for modelling the effect of pharmacological substances as well as for modelling diseased neuron and network conditions.

This paper is organised as follows. Section 2 discusses the HH model for the neurons exhibiting the three distinct firing patterns, along with their parameters. Section 3 explains the two different types of synapses and their interconnections with the HH model. Section 4 introduces the network feedback structure. Section 5 provides simulation results to illustrate the accuracy of the proposed model. Finally, Section 6 summarises the results and discusses future directions. Appendix A clarifies the definition of some basic mathematical operations used in Section 4.

2. HH Model

The HH model is a nonlinear dynamical model that uses the hypothesis that the ionic movement, across the membrane of the neuron through ion-specific channels (gates), is responsible for the generation of action potentials [24]. This ionic movement, that is a result of concentration and potential differences, generates currents across the membrane which are sufficiently strong to cause membrane depolarisation (that is a sudden potential drop) [25]. During the depolarisation phase the membrane ionic permeability, that corresponds to sodium and potassium conductances, changes dramatically to restore the membrane potential leading to a sudden increase in membrane potential, giving the so-called repolarisation phase [26]. The change in membrane permeability is executed via the activation and inactivation processes, the rates and steady state values of which depend on the membrane potential [27].

The original HH model based on measurements from a giant squid axon is only able to fire at fixed time intervals, thus it only exhibits regular spiking patterns. Neurons in the human brain are way more complex in terms of structural and electrophysiological characteristics. In fact, neurons belonging to different brain regions are characterised by extreme firing pattern variability, with some cortical pyramidal cells in the cerebral cortex and hippocampus generating regular spikes, while others exhibiting adaptation or bursting behavior [28]. For the design of the network model, the three most common types of neurons observed in the mammalian brain have been considered: Fast spiking (FS) neurons which are the most common interneurons in the neocortex and are important for the processing of sensory information [29]; excitatory regular spiking with adaptation (RSA) neurons which are the most typical neurons in the cortex [30]; and intrinsic bursting (IB) neurons which are important for motor, sensory and cognitive functions [31]. The goal of incorporating the aforementioned neuronal types in the network model is to reflect some of the large dynamical heterogeneity observed in the mammalian brain and thus be able to simulate a variety of important neuronal processes, such as sensory contrast enhancement and memory.

The neuronal dynamics can all be modeled as an electric circuit (see Fig. 1) with a capacitor C_M as the membrane charge, four variable voltage dependent conductances, g_K, g_M, g_{Na}, and g_{Ca}, as the potassium, slow potassium, sodium and calcium channels, respectively, and the constant conductance g_L modelling the leak chloride channel to include the permeability of the membrane to chloride ions (Cl^-) [32], all connected in parallel. The resting potentials V_K, V_{Na}, V_{Ca} and V_L, which are modeled with three constant voltage sources, are calculated from the concentration based Nerst equation. The injected current (I_{inj}) models an input current to the membrane due to a stimulus from an external source. The activation and inactivation of the potassium, sodium and calcium channels are associated with the dimensionless variables n, m, h, p, q, and s, the values of which are bounded between 0 and 1.

Fast spiking (FS) neurons, which fire at regular faster rate than regular spiking (RS) neurons, can be modeled with sodium (Na^+) and potassium (K^+) gates. In regular spiking with adaptation (RSA) neurons high frequency spikes are followed by lower constant frequency spiking. This can be modeled by the addition of a

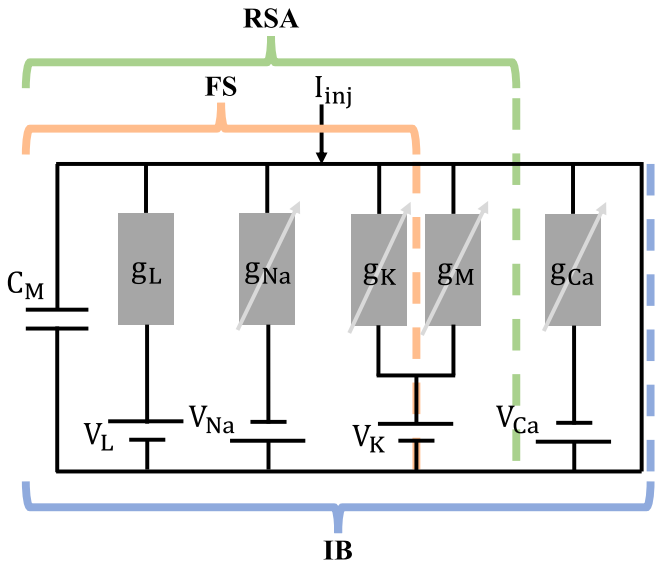

Fig. 1. Electric equivalent of the augmented HH model.

slow non-inactivating potassium (K^+) gate. In intrinsically bursting (IB) neurons, each fast spiking train is followed by a period of quiescence [33]. This can be modeled with the addition of a slow calcium (Ca^{2+}) gate to the original HH model.

The neuron dynamics of an FS neuron are given by the differential equations, adapted from [14]:

$$\begin{cases} \dot{V}(t) = \frac{1}{C_M}\big(I_{inj}(t) - \bar{g}_K n^4(t)(V(t)-V_K) \\ \qquad -\bar{g}_{Na} m^3(t)h(t)(V(t)-V_{Na}) - g_L(V(t)-V_L)\big), \\ \dot{n}(t) = a_n(t)[1-n(t)] - \beta_n n(t), \\ \dot{m}(t) = a_m(t)[1-m(t)] - \beta_m m(t), \\ \dot{h}(t) = a_h(t)[1-h(t)] - \beta_h h(t), \end{cases} \tag{1}$$

in which

$$\begin{cases} a_n(t) = (V(t)-V_T-15)\frac{-0.032}{e^{\left(\frac{-(V(t)-V_T-15)}{5}\right)}-1}, \\ a_m(t) = (V(t)-V_T-13)\frac{-0.32}{e^{\left(\frac{-(V(t)-V_T-13)}{4}\right)}-1}, \\ a_h(t) = 0.128e^{\left(\frac{-(V(t)-V_T-17)}{18}\right)}, \\ \beta_n(t) = 0.5e^{\left(\frac{-(V(t)-V_T-10)}{40}\right)}, \\ \beta_m(t) = 0.28e^{\left(\frac{V(t)-V_T-40}{5}\right)}-1, \\ \beta_h(t) = 4\frac{1}{e^{\left(\frac{-(V(t)-V_T-40)}{5}\right)}+1}. \end{cases} \tag{2}$$

Table 1
HH model variables and definitions.

Variables	Units	Definitions
V	mV	the membrane potential
n, m, h, p, q, s		dimensionless variables with values between 0 and 1 associated with the activation and inactivation of the potassium, sodium and calcium channels
I_{inj}	$\frac{\mu A}{cm^2}$	injected current per unit area

The variable potassium and sodium conductances are $g_K(t) = \bar{g}_K n^4(t)$ and $g_{Na}(t) = \bar{g}_{Na} m^3 h(t)$, respectively, with $\bar{g}_K > 0$ and $\bar{g}_{Na} > 0$ the maximum potassium and sodium conductances, and V_T a threshold adjustment constant associated with FS neurons. The voltage dependent rates of activation and inactivation of the potassium and sodium gates $a_{n,m,h}(t)$ and $\beta_{n,m,h}(t)$ are the result of data fitting from experimental results [14].

Similarly, modelling the neuronal dynamics for an RSA neuron gives the differential equations:

$$\begin{aligned} \dot{V}(t) &= \frac{1}{C_M}\big(I_{inj}(t) - \bar{g}_K n^4(t)(V(t)-V_K) - \bar{g}_M p(t)(V(t)-V_K) \\ &\quad -\bar{g}_{Na} m^3(t)h(t)(V(t)-V_{Na}) - \bar{g}_L(V(t)-V_L)\big), \\ \dot{p}(t) &= \frac{p_\infty(t)-p(t)}{\tau_p(t)}, \end{aligned} \tag{3}$$

where n, m and h are as in Eq. (1), $a_n, \beta_n, a_m, \beta_m, a_h$ and β_h are given in Eq. (2), and

$$\begin{aligned} p_\infty(t) &= \frac{1}{e^{\left(\frac{-(V(t)+35)}{10}\right)}+1}, \\ \tau_p(t) &= \frac{\tau_{max}}{3.3e^{\left(\frac{(V(t)+35)}{20}\right)}+e^{\left(\frac{-(V(t)+35)}{20}\right)}}. \end{aligned} \tag{4}$$

Moreover, the variable slow potassium conductance is $g_M(t) = \bar{g}_M p(t)$, with $\bar{g}_M > 0$ the maximum conductance and $\tau_{max} > 0$ a time constant associated with RSA neurons.

Finally, modelling the neuronal dynamics for an IB neuron gives the differential equations:

$$\begin{cases} \dot{V}(t) = \frac{1}{C_M}\big(I_{inj}(t) - \bar{g}_K n^4(t)(V(t)-V_K) \\ \qquad -\bar{g}_M p(t)(V(t)-V_K) - \bar{g}_{Ca} q^2(t)s(t)(V(t)-V_{Ca}) \\ \qquad -\bar{g}_{Na} m^3(t)h(t)(V(t)-V_{Na}) - \bar{g}_L(V(t)-V_L)\big), \\ \dot{q}(t) = a_q(t)[1-q(t)] - \beta_q(t)q(t), \\ \dot{s}(t) = a_s(t)[1-s(t)] - \beta_s(t)s(t), \end{cases} \tag{5}$$

where n, m and h are as in Eq. (1), $\dot{p}$ is as in Eq. (3), $a_n, \beta_n, a_m, \beta_m, a_h$ and β_h are given in Eq. (2), p_∞ and τ_p are given in Eq. (4) and

$$\begin{cases} a_q(t) = 0.0055(-27-V(t))\frac{1}{e^{\left(\frac{(-27-V(t))}{3.8}\right)}-1}, \\ a_s(t) = 0.000457e^{\left(\frac{(-13-V(t))}{50}\right)}, \\ \beta_s(t) = 0.0065\frac{1}{e^{\left(\frac{(-15-V(t))}{28}\right)}+1}, \\ \beta_q(t) = 0.94e^{\left(\frac{(-75-V(t))}{17}\right)}. \end{cases} \tag{6}$$

The variable calcium conductance is $g_{Ca}(t) = \bar{g}_{Ca} q^2 s(t)$, with $\bar{g}_{Ca}$ the maximum calcium conductance associated with IB neurons. The voltage dependent rates of activation and inactivation of the calcium gate a_q, a_s, β_q and β_s are the result of data fitting from experimental results [14]. The variables involved in the HH models are summarised in Table 1. The HH equations of the IB neurons are able to model the dynamics of both FS and RSA neurons by adjusting the values of the parameters according to Table 2.

Table 2
HH model parameters and values for each neuron type.

Model Parameters	Units	FS	RSA	IB
C_M	$\frac{\mu F}{cm^2}$	0.5	1	1
V_K	mV	−90	−90	−90
V_{Ca}	mV	–	–	120
V_{Na}	mV	50	56	50
V_L	mV	−70	−70.3	−70
V_T	mV	−56.2	−56.2	−56.2
$\bar{g}_K$	$\frac{mS}{cm^2}$	10	6	5
$\bar{g}_M$	$\frac{mS}{cm^2}$	–	0.075	0.03
$\bar{g}_{Ca}$	$\frac{mS}{cm^2}$	–	–	0.2
$\bar{g}_{Na}$	$\frac{mS}{cm^2}$	56	56	50
g_L	$\frac{mS}{cm^2}$	$1.5 \cdot 10^{-2}$	$2.05 \cdot 10^{-2}$	0.01
τ_{max}	$msec$	1	608	608

The injected current $I_{inj}(t)$ can be modeled as a piecewise constant signal as follows:

$$I_{inj}(t) = \begin{cases} rand(a,b), & t \in [0,d], \\ rand(a,b), & t \in [d,2d], \\ \vdots & \vdots \\ rand(a,b), & t \in [(l-1)d, ld], \end{cases}$$

where $rand(a,b) \in \mathbb{R}$ with $0 \leqslant a < b$ is a uniformly distributed random number between a and b, $d = \frac{t}{l}$ is a fixed time step, and l is the number of time partitions, with ld the overall duration of the simulation.

3. Network design

Two neurons can be connected together via an electrical synapse (gap junction) (see Fig. 2A) or via a chemical synapse (see Fig. 2B). Theses two modes of signal propagation in a neuronal network have been proven to coexist in all nervous systems [34]. Each neuron can receive signals from multiple neurons. In electrical signal transmission the axon terminal of the presynaptic neuron (the neuron sending the signal) is in contact with one of the dendrites of the postsynaptic neuron (the neuron receiving the signal). The postsynaptic action potential is directly related to the presynaptic potential. In chemical signal transmission the action potential of the presynaptic neuron activates the release of neurotransmitters in the gap (synaptic cleft) between the presynaptic and postsynaptic neuron. The neurotransmitters activate the receptors of the postsynaptic neuron and a postsynaptic action potential is created that depends on both the presynaptic potential and the neurotransmitter release.

In a network of N neurons the electrical synapse is modeled by the addition of the sum of synaptic currents originating from other neurons to the voltage equation of the HH model as discussed in [35], that is

$$\begin{aligned} \dot{V}_i(t) = \frac{1}{C_M^i}\Big(& I_{inj}^i - \bar{g}_K^i n_i^4(t)\Big(V_i(t) - V_K^i\Big) - \bar{g}_M^i p_i(t)\Big(V_i(t) - V_K^i\Big) \\ & - \bar{g}_{Ca}^i q_i^2(t) s_i(t)\Big(V_i(t) - V_{Ca}^i\Big) - \bar{g}_{Na}^i m_i^3(t) h_i(t)\Big(V_i(t) - V_{Na}^i\Big) \\ & - g_L^i\Big(V_i(t) - V_L^i\Big) + \sum_{j=1}^{N} \epsilon_{ij}^{el}\big(V_j(t) - V_i(t)\big)\Big), \end{aligned} \tag{7}$$

where i is the postsynaptic neuron and j is the presynaptic neuron. The synaptic weight ϵ_{ij}^{el}, that represents the strength of the connection, has unit of conductance. In a network of N neurons, the chemical synapse is modeled by the addition of the sum of synaptic currents originating from other neurons to the voltage equation of the original HH model as discussed in [35,7], that is

$$\begin{aligned} \dot{V}_i(t) = \frac{1}{C_M^i}\Big(& I_{inj}^i - \bar{g}_K^i n_i^4(t)\Big(V_i(t) - V_K^i\Big) - \bar{g}_M^i p_i(t)\Big(V_i(t) - V_K^i\Big) \\ & - \bar{g}_{Ca}^i q_i^2(t) s_i(t)\Big(V_i(t) - V_{Ca}^i\Big) - \bar{g}_{Na}^i m_i^3(t) h_i(t)\Big(V_i(t) - V_{Na}^i\Big) \\ & - g_L^i\Big(V_i(t) - V_L^i\Big) + \sum_{j=1}^{N} \epsilon_{ij}^{ch} r_j\Big(V_{syn}^i - V_j(t)\Big)\Big)\Big), \end{aligned} \tag{8}$$

where i is the postsynaptic neurons, j is the presynaptic neuron, and V_{syn}^i is the reversal potential of the synapse. In this case the synaptic weight ϵ_{ij}^{ch} is unit-less. In both Eq. (7) and Eq. (8), the synaptic weights ϵ_{ij} conventionally correspond to the effect of neuron j on neuron i.

Finally, the fraction of receptors r bound to the neurotransmitters [36] is described by

$$\dot{r}_j(t) = \left(\frac{1}{\tau_r} - \frac{1}{\tau_d}\right)\frac{(1 - r_j(t))}{1 + e^{-V_j(t)+V_0}} - \frac{1}{\tau_d} r_j(t), \tag{9}$$

in which V_0 is the reversal potential, τ_d is the decay time constant, and τ_r is the rise time constant [35], the values of which are given in Table 3.

Table 3
Synapse parameters and values for each neuron type.

Synapse Parameters	Units	FS	RSA	IB
τ_r	$msec$	0.5	0.5	0.5
τ_d	$msec$	8	8	8
V_{syn}	mV	$[-80,-50]$	20	20
V_0	mV	-20	-20	-20

4. Feedback Structure

Graph theory has been used extensively for the understanding of complex neuronal networks in terms of structure and functionality, see e.g. [17]. In a graph theory based approach, the individual neurons correspond to the nodes of the graph, illustrated by solid dots. The coupling between neurons is represented by the edges, i.e lines connecting the neurons. A neuronal network can ideally be represented by a directed weighted graph, in which each edge is paired with a non-negative synaptic weight ϵ_{ij}, to illustrate the effect of neuron j on neuron i.

As previously mentioned, there are two distinct ways in which neurons can communicate with each another: electrical and chemical signal transmission. In what follows we present a novel compact formalism for these two types of networks.

To begin with, we consider a network of neurons, connected with electrical coupling with strength $\epsilon^{el} \geqslant 0$, of size N. We define

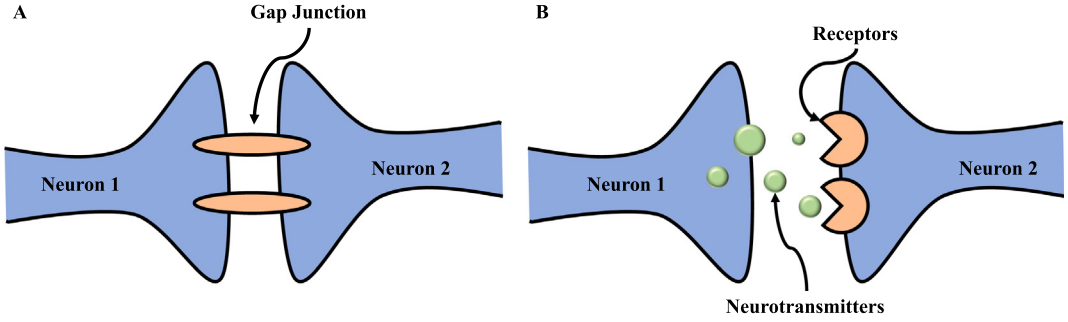

Fig. 2. Coupling between two neurons with electrical (A) and chemical (B) synapses.

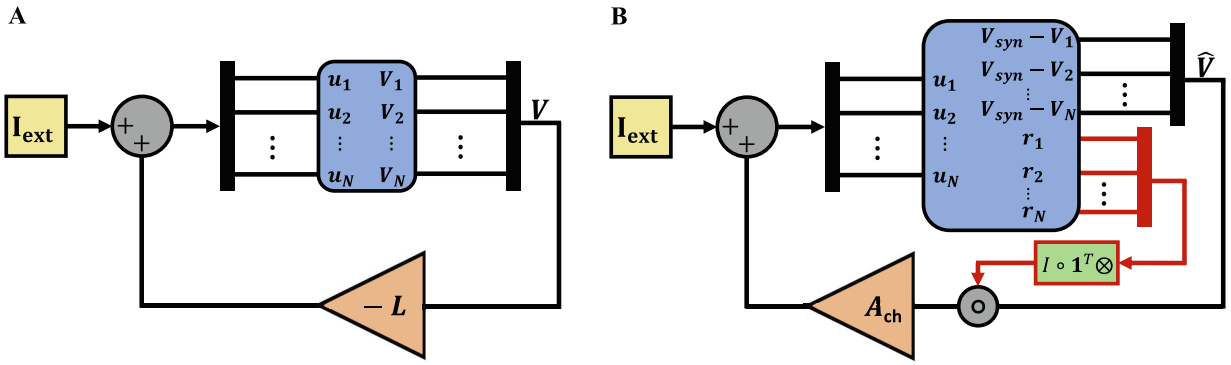

Fig. 3. Feedback Structure of a neuronal network with electrical (A) and chemical (B) coupling.

the adjacency matrix A_{el} that is populated with the coupling strengths between connected neurons. We do not consider the case of self-coupling as, consistent with our mathematical framework we only account for autapses performed by chemical synapses, thus the diagonal is filled with zeros. We also define the diagonal degree matrix D in which each element is the sum of the corresponding row of the adjacency matrix. The matrices are of dimension $N \times N$, and are given by the expressions

$$A_{el} = \begin{bmatrix} 0 & \epsilon_{12}^{el} & \dots & \epsilon_{1N}^{el} \\ \epsilon_{21}^{el} & \ddots & & \vdots \\ \vdots & & \ddots & \vdots \\ \epsilon_{N1}^{el} & \dots & \dots & 0 \end{bmatrix},$$

$$D = \begin{bmatrix} \sum_{j=1}^{N} \epsilon_{1j}^{el} & 0 & \dots & 0 \\ 0 & \sum_{j=1}^{N} \epsilon_{2j}^{el} & 0 & \vdots \\ \vdots & 0 & \ddots & \vdots \\ 0 & \dots & \dots & \sum_{j=1}^{N} \epsilon_{Nj}^{el} \end{bmatrix},$$

where, consistently with our assumptions, $\epsilon_{ii} = 0$. We then define the Laplacian matrix L, which provides the matrix form of the graph, as

$$L = D - A_{el} = \begin{bmatrix} \sum_{j=1}^{N} \epsilon_{1j}^{el} & -\epsilon_{12}^{el} & \dots & -\epsilon_{1N}^{el} \\ -\epsilon_{21}^{el} & \sum_{j=1}^{N} \epsilon_{2j}^{el} & \dots & \vdots \\ \vdots & \vdots & \ddots & \vdots \\ -\epsilon_{N1}^{el} & \dots & \dots & \sum_{j=1}^{N} \epsilon_{Nj}^{el} \end{bmatrix}.$$

If we consider each synaptic current as an input, Eq. (7), for $i,j = 1 \dots N$, can be rewritten in vector form as

$$\begin{aligned} \dot{V}(t) = 1 \oslash C_M \circ \big(& I_{ext} - \bar{g}_K \circ n^{\circ 4}(t) \circ (V(t) - V_K) \\ & - \bar{g}_M \circ p(t) \circ (V(t) - V_K) - \bar{g}_{Ca} \circ q^{\circ 2}(t) \circ s(t) \circ (V(t) - V_{Ca}) \\ & - \bar{g}_{Na} \circ m^{\circ 3}(t) \circ h(t) \circ (V(t) - V_{Na}) - g_L \circ (V(t) - V_L) + u_{el} \big), \end{aligned} \tag{10}$$

where $\oslash$ denotes the Hadamard division and $\circ$ the Hadamard product or power (see Appendix A). The model parameters are the vectors $C_M \in \mathbb{R}^{N\times 1}, \bar{g}_K \in \mathbb{R}^{N\times 1}$, $\bar{g}_M \in \mathbb{R}^{N\times 1}, \bar{g}_{Ca} \in \mathbb{R}^{N\times 1}, \bar{g}_{Na} \in \mathbb{R}^{N\times 1}$, and $g_L \in \mathbb{R}^{N\times 1}$. The current due to the electrical synapses formed between the neurons of the network is defined via the feedback $u_{el} = -LV$ where $V = [\underbrace{V_1, \dots, V_{N_{FS}}}_{FS}, \underbrace{V_{N_{FS+1}}, \dots, V_{N_{FS}+N_{RSA}}}_{RSA}, \underbrace{V_{N_{FS}+N_{RSA}+1}, \dots, V_N}_{IB}]^T$. The rest of the variables and parameters of the model follow the same pattern as the vector V to compactly represent the three different types of neurons that exist in the network, e.g. $C_M = [\underbrace{C_{M,1}, \dots, C_{M,N_{FS}}}_{FS}, \underbrace{C_{M,N_{FS+1}}, \dots, C_{M,N_{FS}+N_{RSA}}}_{RSA}, \underbrace{C_{M,N_{FS}+N_{RSA}+1}, \dots, C_{M,N}}_{IB}]^T$.

The external current $I_{ext} = \mathbf{S} \circ I_{inj} \in \mathbb{R}^{N\times 1}$ is the input vector and $\mathbf{S} \in \mathbb{R}^{N\times 1}$ is a selection column vector that determines which of the neurons receive it. The feedback structure of the network is illustrated in Fig. 3A.

Similarly, for the study of a network based on chemical interactions of strength $\epsilon^{ch} \geqslant 0$ we define the adjacency matrix, this time considering the possibility of self loops, as

$$A_{ch} = \begin{bmatrix} \epsilon_{11}^{ch} & \epsilon_{12}^{ch} & \dots & \epsilon_{1N}^{ch} \\ \epsilon_{21}^{ch} & \ddots & & \vdots \\ \vdots & & \ddots & \vdots \\ \epsilon_{N1}^{ch} & \dots & \dots & \epsilon_{NN}^{ch} \end{bmatrix},$$

and the vectors $\widehat{V} = [V_{syn} - V_1, \dots, V_{syn} - V_N]^T$ and $\mathbf{r} = [r_1, \dots, r_N]^T$. Eq. (8), for $i,j = 1 \dots N$, is then rewritten in vector form as

$$\begin{aligned} \dot{V}(t) = 1 \oslash C_M \circ \big(& I_{ext} - \bar{g}_K \circ n^{\circ 4}(t) \circ (V(t) - V_K) \\ & - \bar{g}_M \circ p(t) \circ (V(t) - V_K) - \bar{g}_{Ca} \circ q^{\circ 2}(t) \circ s(t) \circ (V(t) - V_{Ca}) \\ & - \bar{g}_{Na} \circ m^{\circ 3}(t) \circ h(t) \circ (V(t) - V_{Na}) - g_L \circ (V(t) - V_L) + u_{ch} \big), \end{aligned} \tag{11}$$

with feedback $u_{ch} = A_{ch}\left(I_N \circ \left(\mathbf{1}^T \otimes r\right) \circ \widehat{V}\right)$, where $\otimes$ denotes the Kronecker product (see Appendix A) and and $\mathbf{1}$ is a column vector of ones and dimension N. The feedback structure of the network is illustrated in Fig. 3B.

For the modelling of an heterogeneous network with both electrical and chemical synapses present, all neuron parameters are considered known (see Table 2), while the network design parameters, which are the external current I_{ext}, the selection vector S and the adjacency matrices A_{el} and A_{ch} are network-specific. In this case the feedback takes the form of $u = u_{el} + u_{ch} = -LV + A_{ch}\left(I_N \circ \left(\mathbf{1}^T \otimes r\right) \circ \widehat{V}\right)$. The choice of including electrical and/or chemical synapses is biologically motivated and does not affect the design procedure. If only one type of synapse exists in the modelled network the adjacency matrix corresponding to the absent synapse must be filled with zeros. In any case, the performance of the network design depends on the size of the network. The feedback due to the electrical synapses only depends on the output

vector V, while the feedback due to the chemical synapse depends both on the error vector $\hat{V}$ and the variable r. This difference in the form of the feedback is based on the different biological processes associated with the two modes of coupling.

The adoption of the feedback structure in the HH network model achieves the separation of the neuron and network dynamics and provides a simplified compact and straightforward vectorised formalism for the network equations that is easily scalable to accommodate any size of network. The separation of the neuron and network dynamics is achieved via the vectorisation of the network equations, the incorporation of the feedback law and the description of the neuron interactions via the corresponding connectivity matrices.

5. Model validation

The performance and robustness of neuronal brain networks is based on the function of some fundamental neuron motifs (see Fig. 4). Those small networks are the building blocks of bigger neuronal circuits and are responsible for essential functions such as encoding, representation and computation [37]. Despite their presence and their significant impact on the behaviour of large neuronal networks in mammalian brains there is a lack of visual portrayal of their individual and global activity in the literature. In what follows, we use our proposed framework to simulate the activity of those neuronal circuits and correlate them to their respective functions.

First we consider three uncoupled neurons with distinct firing patters, FS, RSA and IB, all receiving external input (Fig. 5). It can be observed that the FS neurons fire faster and more erratically than the RSA neurons, while the IB neurons exhibit fast spiking trains alternated by periods of quiescence. The variability of the input current in each of the neurons prevents any periodicity of the resulting voltages. After the current is no longer applied the neurons return to their equilibrium.

5.1. Feedforward and feedback excitation

Feedforward excitation (Fig. 4A) facilitates the propagation of information from one neuron to another, while the feedback excitation (Fig. 4B) sustains the activation of the presynaptic neuron using the output of the postsynaptic neuron [38]. To simulate feedforward excitation we have designed a network of two excitatory RSA neurons coupled with an electrical synapse ($\epsilon_{21}^{el} = 0.1\,mS$) with only the first neuron receiving external input (Fig. 4A). We observe that the postsynaptic neuron 2 fires solely because of its connection to the presynaptic neuron 1 (Fig. 6A) and in accordance with the synaptic strength between the two neurons proving the forward relay of information. The magnitude of the synaptic coupling determines the level of dependence of neuron 2 on neuron 1 and is responsible, in this example, for the different number of occurred spikes. Keeping the external input the same, we have added a feedback chemical synapse ($\epsilon_{12}^{ch} = 0.5$) from neuron 2 to neuron 1 (Fig. 4B). As a result of the feedback connection both neurons exhibit increased activity in the form of high frequency spiking trains (Fig. 6B). The significance of the feedback connection is displayed in the ability of neuron 1 to indirectly increase its individual activity under the same external input.

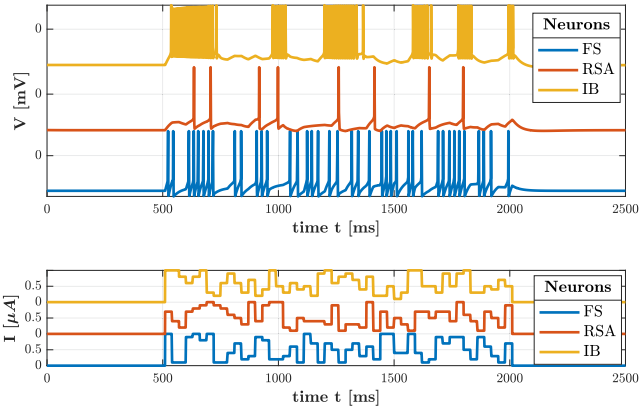

Fig. 5. Simulation results for 3 uncoupled FS, RSA and IB neurons all receiving external input. The external current is applied from 500 *msec* up to 2000 *msec* with maximum amplitude $1\mu A$.

5.2. Feedforward and feedback inhibition

Feedforward inhibition (Fig. 4C) limits or completely shuts down the activity of a postsynaptic neuron. Feedback inhibition (Fig. 4D) limits the excitation of a neuron via the activation of the inhibitory neuron. To demonstrate the effect of feedforward

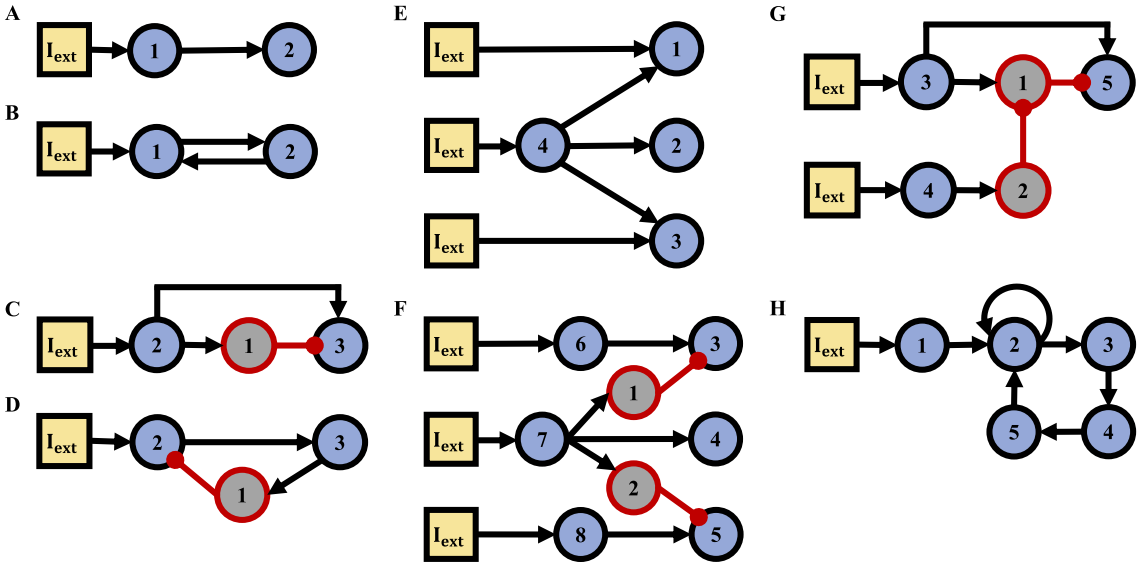

Fig. 4. Important neuron motifs commonly observed in brain circuits: (A) Feedforward excitation, (B) feedback excitation, (C) feedforward inhibition, (D) feedback inhibition, (E) lateral excitation, (F) lateral inhibition, (G) disinhibition and (H) recurrent excitation. Blue neurons are excitatory and grey neurons are inhibitory. Adapted from [37].

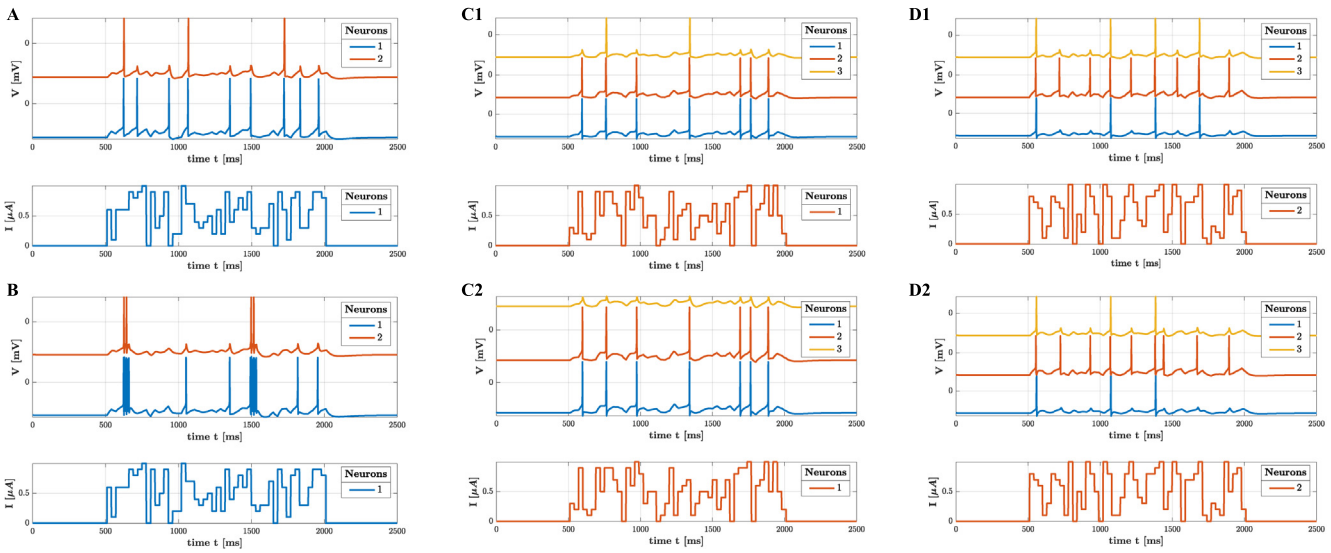

Fig. 6. Simulation results for: (A) feedforward excitation, (B) feedback excitation, (C1-C2) feedforward inhibition and (D1-D2) feedback inhibition circuits.

inhibition we have designed a network of two excitatory RSA neurons and one inhibitory FS neuron (Fig. 4C). First, we consider the case in which connection between the inhibitory neuron 1 and the excitatory neuron 2 is disabled and the remaining circuit is feedforward excitation from neuron 2 to neuron 3 coupled with an electrical synapse ($\epsilon^{el}_{32} = 0.1\,mS$) and from neuron 2 to neuron 1 coupled with an electrical synapse ($\epsilon^{el}_{12} = 0.2\,mS$). In this case, neurons 1 and 3 fire because of their connection to neuron 2, the only neuron that receives external input (Fig. 6C1). The neurons 1 and 3 fire with different frequencies because of the different synaptic strengths (neuron 1 is more heavily affected by neuron 2). If the inhibitory chemical synapse between neurons 1 and 3 is enabled ($\epsilon^{ch}_{31} = 0.05$), the excitation of neuron 3 is completely shut down by the inhibitory effect of neuron 1 and results in total quiescence (Fig. 6C2). The inability of neuron 3 to fire demonstrates the ability of an inhibitory neuron to terminate the activity of a postsynaptic neuron and therefore accurately depicts the function of a feedforward inhibition circuit.

Similarly, to illustrate the function of feedback inhibition we have designed a network of two excitatory RSA neurons and one inhibitory FS neuron (Fig. 4D). In this case, neuron 1 is excited by neuron 3 via an electrical synapse ($\epsilon^{el}_{13} = 0.1\,mS$), which in turn is excited by neuron 2 via an electrical synapse ($\epsilon^{el}_{32} = 0.1\,mS$). When the inhibitory synaptic connection between neurons 1 and 2 is disabled all neurons successfully fire because of neuron 2 receiving external input and their respective connections (Fig. 6D1). If the inhibitory chemical synapse between neurons 1 and 2 is enabled ($\epsilon^{ch}_{21} = 0.1$), the activity of the output neuron 3 is limited because of the feedback inhibition (Fig. 6D2). The biggest difference between the two networks lies on the extent of efficacy of the inhibitory neuron to silence the output of neuron 3 as well as on its effect on the whole network. Feedforward excitation is able to completely shut down the activity of the output neuron while maintaining the activity of the rest of the neurons in the network, whereas feedback excitation is only able to cap the relay of information to the output neuron via the limited activity of all the neurons in the network.

5.3. Lateral excitation and lateral inhibition

Lateral excitation (Fig. 4E) amplifies the sensitivity of the neurons to an external input current [39]. On the other hand, lateral inhibition (Fig. 4F) is very important in edge detection as it increases the contrast between different levels of visual stimulus at the boundary [40,41]. To simulate lateral excitation we have designed a network of four RSA neurons connected with electrical ($\epsilon^{el}_{24} = 0.1\,mS$) and chemical ($\epsilon^{ch}_{14} = 0.1, \epsilon^{ch}_{34} = 0.1$) synapses with all neurons except neuron 2 receiving external input (Fig. 4E). If the strengths of the two chemical synapses are set to zero, therefore neuron 4 has no effect upon neurons 1 and 3, all neurons fire driven by their respective external and synaptic input (Fig. 7E1). If the two chemical synapses are enabled neurons 1 and 3 exhibit increased activity (Fig. 7E2) under the same input current. This circuit establishes some sort of communication between the neurons 4, 1 and 3 in which neuron 4 dictates the level of sensitivity of neurons 1 and 3 to their respective inputs. We have repeated the simulation for four IB neurons and the behaviour of the circuit is consistent with the previous results (Fig. 7E3 and Fig. 7E4).

To demonstrate the effect of lateral inhibition we have designed a network with six RSA and two FS neurons connected with electrical ($\epsilon^{el}_{36} = \epsilon^{el}_{17} = \epsilon^{el}_{27} = \epsilon^{el}_{58} = 0.1\,mS$) and chemical ($\epsilon^{ch}_{31} = \epsilon^{ch}_{52} = 0.2$) synapses. If the two chemical synapses are disabled ($\epsilon^{ch}_{31} = \epsilon^{ch}_{52} = 0$), neurons 3 and 5 fire driven by the external input received by neurons 6 and 8, respectively (Fig. 7F1). If the two chemical synapses are enabled, neurons 3 and 5 exhibit decreased firing activity because of the inhibition of neurons 1 and 2 (Fig. 7F2). The number of spikes of neurons 3, 4 and 5 are indicators of the intensities of the input currents with smaller number of spikes corresponding to lower input current. By observing the behaviour of the neurons it becomes clear that the circuit amplifies the distinction between the neurons receiving different levels of input current, in other words increases their contrast.

5.4. Disinhibition

Disinhibition (Fig. 4G) breaks the balance of excitation/inhibition and is an important mechanism often observed in learning and memory [42]. To demonstrate the effect of disinhibition we have designed a network of three RSA and two FS neurons connected with electrical ($\epsilon^{el}_{13} = 0.05\,mS, \epsilon^{el}_{53} = \epsilon^{el}_{24} = 0.1\,mS$) and chemical ($\epsilon^{ch}_{51} = \epsilon^{ch}_{12} = 0.05$) synapses. If the chemical synapse from neuron 2 to neuron 1 is disabled ($\epsilon^{ch}_{12} = 0$), the activity of neuron 5 is shut down by the inhibitory neuron 1 despite the excitation it receives from neuron 3 (Fig. 8G1). If the same chemical synapse

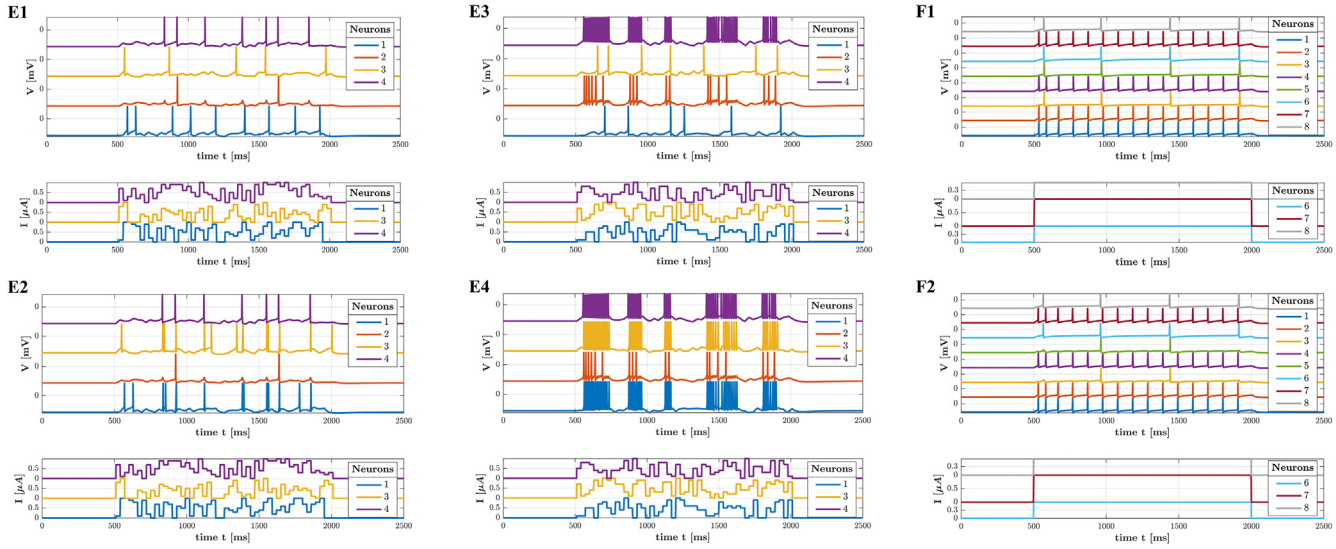

Fig. 7. Simulation results for: (E1-E4) lateral excitation and (F1-F2) lateral inhibition circuits.

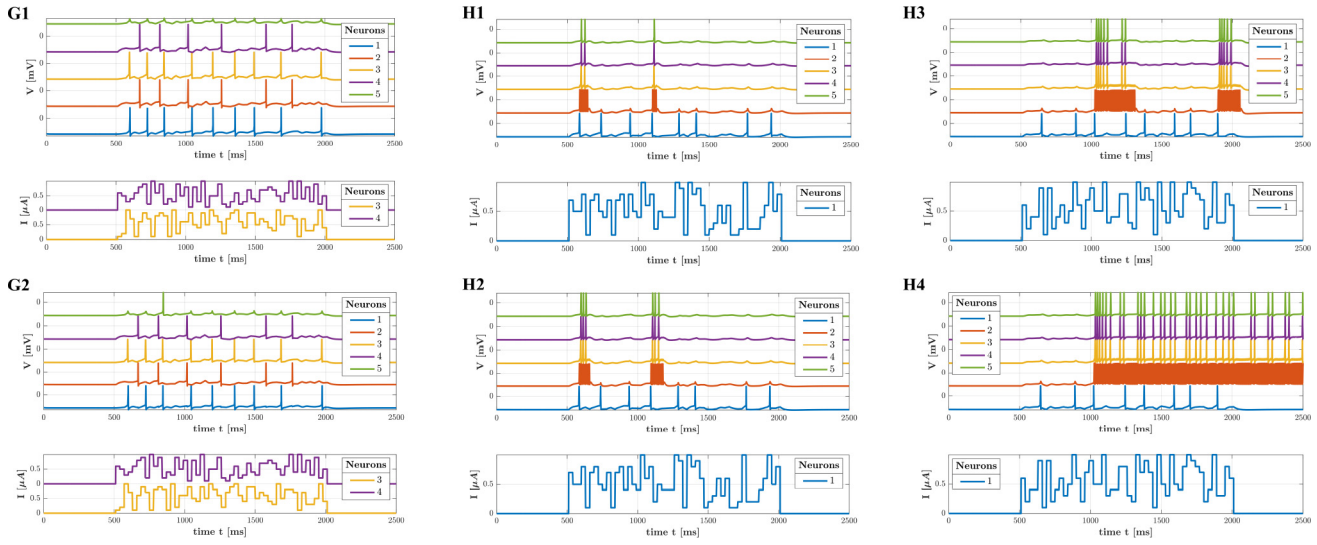

Fig. 8. Simulation results for: (G1-G2) disinhibition, (H1-H4) recurrent excitation circuits.

is enabled, neuron 2 inhibits the inhibitory neuron 1 thus limiting its effect on neuron 5 which in this cases fires (Fig. 8G2). Disinhibition acts as a conditional switch between the activity or quiescence of the output neuron based on the input currents and coupling strengths and describes a very important function in many neuronal circuits.

5.5. Recurrent excitation

Recurrent excitation (Fig. 4H) generates bistability between two states: spontaneous activity in the frequency range $0-10$ *Hz* and persistent activity in the tens of *Hz* frequency range once the stimulus is removed [43]. To simulate the function of recurrent excitation we have designed a network of five RSA neurons connected with electrical $(\epsilon_{21}^{el}=\epsilon_{32}^{el}=0.1\,mS, \epsilon_{43}^{el}=\epsilon_{54}^{el}=0.1mS)$ and chemical $(\epsilon_{22}^{ch}=\epsilon_{25}^{ch}=0.15)$ synapses. Without the feedback $(\epsilon_{25}^{ch}=0)$ the circuit is simply an in-series connection of neurons 1–5 and a self-loop (Fig. 8H1). With the addition of the connection between neurons 1 and 5, all neurons except neuron 1 demonstrate increased firing activity (Fig. 8H2) as a result of the recurrent feedback. We have repeated the simulation with different input current and chemical synaptic strength pairs $(\epsilon_{22}^{ch}=0.18, \epsilon_{25}^{ch}=0.2)$ and $(\epsilon_{22}^{ch}=0.2, \epsilon_{25}^{ch}=0.2)$ to produce Fig. 8H3 and Fig. 8H4, respectively. Recurrent feedback takes the form of the self loop on neuron 2 as well as the form of feedback from neuron 5 to neuron 2. The aforementioned simulations demonstrate how recurrent feedback generates bistability between low and high frequency firing which persists after the removal of the external current at $2000\,ms$.

5.6. Random large-scale network

As highlighted in the preceding discussion, the proposed model reliably describes the dynamics of basic small networks consisting of different types of neurons and synapses with high flexibility. To prove its scalability we have modeled large networks with random connectivity, synaptic strengths, external currents and input selection vectors. Three homogeneous modules composed of FS, RSA and IB neurons have been interconnected to demonstrate the effect of random interconnection on a large-scale network. Fig. 9A illustrates a network of 30 FS, 90 RSA and 30 IB neurons randomly

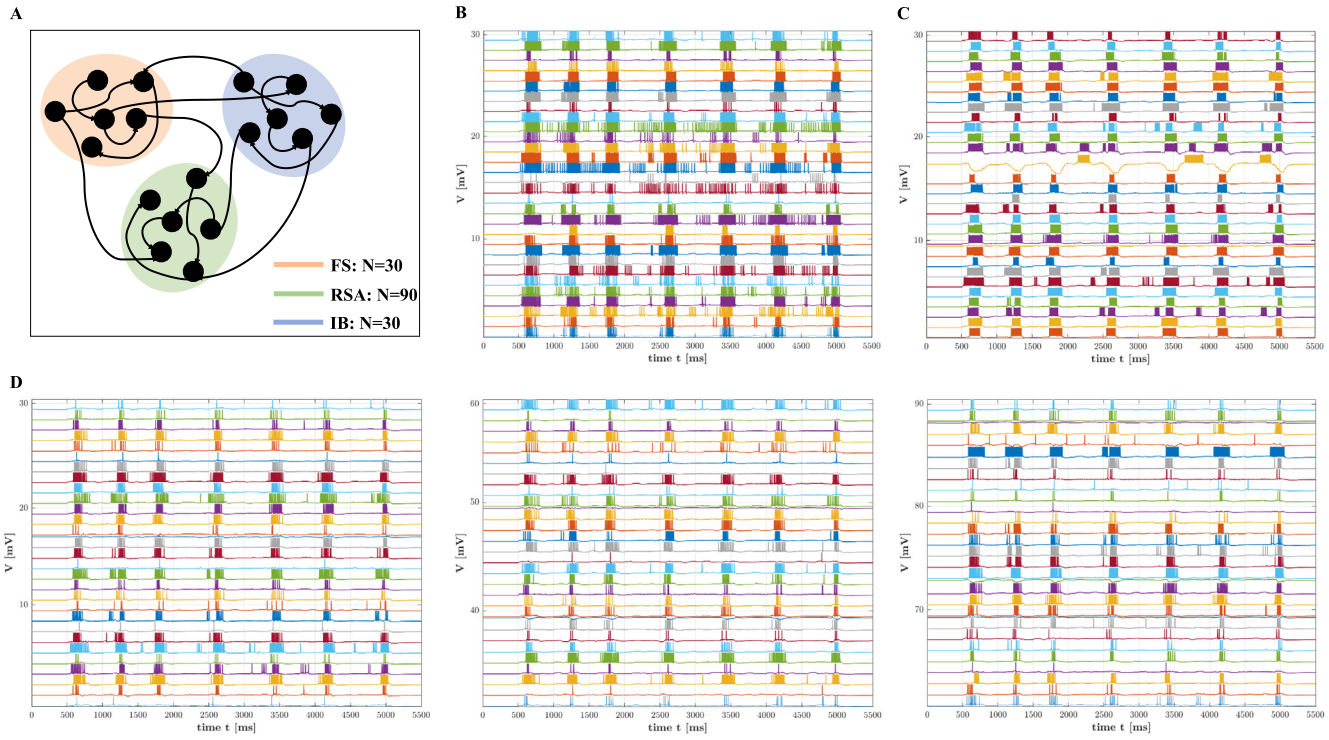

Fig. 9. Random network: (A) schematic representation of a random network with 30 FS, 90 RSA and 30 IB neurons, (B) voltage traces of FS neurons, (C) voltage traces of IB neurons, (D) voltage traces of RSA neurons in groups of 30.

interconnected with synaptic strengths ranging from 0 to 0.06 mS for the electrical synapses and from 0 to 0.1 for the chemical synapses. The input currents are random piecewise functions with maximum amplitude 0.1 μA. The activity of the individual neurons, which depends on the external and synaptic inputs, is presented in Fig. 9(B-D).

6. Conclusion

We have presented a novel scalable, adaptable and modular modelling framework based on a compact feedback structure that is able to model networks of heterogeneous Hodgkin–Huxley neurons interconnected via electrical and chemical synapses. The model is able to reproduce the activity of neuronal networks subject to the presence of external input currents. The separation of the individual neuron and network dynamics makes this model adaptable and easily expandable to incorporate more types of neurons, synapses and network structures. We have validated the efficacy of the model by simulating a few basic important neuronal circuits that perform specific functions and are the basis of bigger neuronal networks commonly observed in mammalian brains. We have demonstrated the scalability of the model by adding an example of a larger random network and we have provided all the necessary parameter values to maximize the reproducibility of the results. With this work we aim to simplify the process of simulating neuronal networks by providing a compact, flexible and scalable modelling framework that can be adjusted and/or expanded with ease. The ability of the proposed modelling framework to produce the activity of large heterogeneous neuronal networks is indicative of its potential use for educational and research purposes.

As future development we aim to simulate modular and small-world networks that are thought to be present in the mammalian brain circuitry. We plan to investigate the robustness of the model under various neuron and network parameter changes. Furthermore, we will investigate the effect of individual neurons or synaptic connections failing in an attempt to simulate the effects of Alzheimer's and Parkinson's disease on the functionality of networks. Finally, we aim to apply control and consensus theory to potentially repair any broken pathways and maintain the network performance.

CRediT authorship contribution statement

A.G. Giannari: Conceptualization, Methodology, Software, Validation, Formal analysis, Writing - original draft, Visualization. **A. Astolfi:** Conceptualization, Validation, Writing - review & editing, Supervision.

Declaration of Competing Interest

The authors declare that they have no known competing financial interests or personal relationships that could have appeared to influence the work reported in this paper.

Acknowledgment

This work was partially supported by the European Union's Horizon 2020 Research and Innovation Program under Grant 739551 (KIOS Centre of Excellence).

Appendix A

Definition 1. The Hadamard product of two matrices with the same dimensions $A = [a_{ij}] \in \mathbb{R}^{m\times n}$ and $B = [b_{ij}] \in \mathbb{R}^{m\times n}$ is defined as $A \circ B = [a_{ij}b_{ij}] \in \mathbb{R}^{m\times n}$ [44].

Definition 2. The Hadamard division or element-wise division of two matrices with the same dimensions $A = [a_{ij}] \in \mathbb{R}^{m\times n}$ and $B = [b_{ij} \neq 0] \in \mathbb{R}^{m\times n}$ is defined by $A \oslash B = [a_{ij}/b_{ij}] \in \mathbb{R}^{m\times n}$ [45].

Definition 3. The Hadamard power of a matrix $A = [a_{ij}] \in \mathbb{R}^{m\times n}$ is defined by $A^{\circ k} = \left[a_{ij}^{k}\right] \in \mathbb{R}^{m\times n}$ with $k \in \mathbb{R}$ and $a_{ij} > 0$ [46].

Definition 4. The Kronecker product of two matrices $A = [a_{ij}] \in \mathbb{R}^{m\times n}$ and $B = [b_{ij}] \in \mathbb{R}^{p\times q}$ gives the block matrix $A \otimes B = \begin{bmatrix} a_{11}B & \dots & a_{1n}B \\ \vdots & \ddots & \vdots \\ a_{m1}B & \dots & a_{mn}B \end{bmatrix} \in \mathbb{R}^{pm\times qn}$ [47].

References

[1] A.L. Hodgkin, A.F. Huxley, A quantitative description of membrane current and its application to conduction and excitation in nerve, The Journal of physiology 117 (1952) 500–544.
[2] Q. Kang, B. Huang, M. Zhou, Dynamic behavior of artificial hodgkin–huxley neuron model subject to additive noise, IEEE Transactions on Cybernetics 46 (2015) 2083–2093.
[3] Y. Xie, L. Chen, Y.M. Kang, K. Aihara, Controlling the onset of Hopf bifurcation in the Hodgkin-Huxley model, Physical Review E 77 (2008) 061921.
[4] J. Guckenheimer, R.A. Oliva, Chaos in the Hodgkin-Huxley model, SIAM Journal on Applied Dynamical Systems 1 (2002) 105–114.
[5] A. Torcini, S. Luccioli, T. Kreuz, Coherent response of the hodgkin–huxley neuron in the high-input regime, Neurocomputing 70 (2007) 1943–1948.
[6] M. Uzuntarla, J.J. Torres, A. Calim, E. Barreto, Synchronization-induced spike termination in networks of bistable neurons, Neural Networks 110 (2019) 131–140.
[7] C.A.S. Batista, R.L. Viana, S.R. Lopes, A.M. Batista, Dynamic range in small-world networks of hodgkin–huxley neurons with chemical synapses, Physica A: Statistical Mechanics and its Applications 410 (2014) 628–640.
[8] K. Pal, D. Ghosh, G. Gangopadhyay, Synchronization and metabolic energy consumption in stochastic hodgkin-huxley neurons: patch size and drug blockers, Neurocomputing 422 (2021) 222–234.
[9] Y. Xu, Y. Jia, M. Ge, L. Lu, L. Yang, X. Zhan, Effects of ion channel blocks on electrical activity of stochastic hodgkin–huxley neural network under electromagnetic induction, Neurocomputing 283 (2018) 196–204.
[10] S. Valadez-Godínez, H. Sossa, R. Santiago-Montero, On the accuracy and computational cost of spiking neuron implementation, Neural Networks 122 (2020) 196–217.
[11] E.M. Izhikevich, Which model to use for cortical spiking neurons?, IEEE Transactions on Neural Networks 15 (2004) 1063–1070
[12] Y. Tsubo, T. Kaneko, S. Shinomoto, Predicting spike timings of current-injected neurons, Neural Networks 17 (2004) 165–173.
[13] Q. Shi, H. Fang, Z. Wang, C. Li, Rhythmic oscillations of excitatory bursting Hodkin-Huxley neuronal network with synaptic learning, Computational Intelligence and Neuroscience (2016).
[14] M. Pospischil, M. Toledo-Rodriguez, C. Monier, Z. Piwkowska, T. Bal, Y. Frégnac, H. Markram, A. Destexhe, Minimal Hodgkin-Huxley type models for different classes of cortical and thalamic neurons, Biological cybernetics 99 (2008) 427–441.
[15] C.J. Stam, J.C. Reijneveld, Graph theoretical analysis of complex networks in the brain, Nonlinear Biomedical Physics 1 (2007) 1–19.
[16] O. Sporns, Graph theory methods: applications in brain networks, Dialogues in clinical neuroscience 20 (2018) 111.
[17] D. Mears, H.B. Pollard, Network science and the human brain: using graph theory to understand the brain and one of its hubs, the amygdala, in health and disease, Journal of Neuroscience Research 94 (2016) 590–605.
[18] D.S. Bassett, P. Zurn, J.I. Gold, On the nature and use of models in network neuroscience, Nature Reviews Neuroscience 19 (2018) 566–578.
[19] M.L. Hines, N.T. Carnevale, The neuron simulation environment, Neural computation 9 (1997) 1179–1209.
[20] P. Gleeson, V. Steuber, R.A. Silver, neuroconstruct: a tool for modeling networks of neurons in 3d space, Neuron 54 (2007) 219–235.
[21] D.F.M. Goodman, R. Brette, The brian simulator, Frontiers in neuroscience 3 (2009) 26.
[22] I.N.C.F. Secretariat, M. Djurfeldt, A. Lansner, 1st incf workshop on large-scale modeling of the nervous system, F1000Research 7 (2018) 1401.
[23] M. Pan, P.J. Gawthrop, J. Cursons, E.J. Crampin, Modular assembly of dynamic models in systems biology, PLoS Computational Biology 17 (2021) e1009513.
[24] A.L. Hodgkin, A.F. Huxley, The components of membrane conductance in the giant axon of Loligo, The Journal of Physiology 116 (1952) 473–496.
[25] A.L. Hodgkin, A.F. Huxley, B. Katz, Measurement of current-voltage relations in the membrane of the giant axon of Loligo, The Journal of Physiology 116 (1952) 424–448.
[26] A.L. Hodgkin, A.F. Huxley, The dual effect of membrane potential on sodium conductance in the giant axon of loligo, The Journal of Physiology 116 (1952) 497–506.
[27] A.L. Hodgkin, A. Huxley, Currents carried by sodium and potassium ions through the membrane of the giant axon of Loligo, The Journal of Physiology 116 (1952) 449–472.
[28] D.A. McCormick, Membrane Potential and Action Potential, in: John H. Byrne, Ruth Heidelberger, M. Neal Waxham (Eds.), From Molecules to Networks, 3rd edition,,, Academic Press, 2014, pp. 351–376.
[29] B. Wang, W. Ke, J. Guang, G. Chen, L. Yin, S. Deng, Q. He, Y. Liu, T. He, R. Zheng, et al., Firing frequency maxima of fast-spiking neurons in human, monkey, and mouse neocortex, Frontiers in Cellular Neuroscience 10 (2016) 239.
[30] E.M. Izhikevich, Simple model of spiking neurons, IEEE Transactions on Neural Networks 14 (2003) 1569–1572.
[31] D.M. Fox, H.G. Rotstein, F. Nadim, Bursting in Neurons and Small Networks, Springer, New York, 2013, pp. 1–17.
[32] H.B. Steinbach, Chloride in the giant axons of the squid, Journal of Cellular and Comparative Physiology 17 (1941) 57–64.
[33] F.A.S. Ferrari, R.L. Viana, S.R. Lopes, R. Stoop, Phase synchronization of coupled bursting neurons and the generalized kuramoto model, Neural Networks 66 (2015) 107–118.
[34] A.E. Pereda, Electrical synapses and their functional interactions with chemical synapses, Nature Reviews Neuroscience 15 (2014) 250–263.
[35] Y. Hao, Y. Gong, L. Wang, X. Ma, C. Yang, Single or multiple synchronization transitions in scale-free neuronal networks with electrical or chemical coupling, Chaos, Solitons & Fractals 44 (2011) 260–268.
[36] A. Destexhe, Z.F. Mainen, T.J. Sejnowski, An efficient method for computing synaptic conductances based on a kinetic model of receptor binding, Neural Computation 6 (1994) 14–18.
[37] J.H. Byrne, R. Heidelberger, M.N. Waxham, From molecules to networks: an introduction to cellular and molecular neuroscience, Academic Press, 2014, Chapter 19, page 576.
[38] M.J. Hull, S.R. Soffe, D.J. Willshaw, A. Roberts, Modelling feedback excitation, pacemaker properties and sensory switching of electrically coupled brainstem neurons controlling rhythmic activity, PLoS Computational Biology 12 (2016) e1004702.
[39] J.M. Christie, G.L. Westbrook, Lateral excitation within the olfactory bulb, Journal of Neuroscience 26 (2006) 2269–2277.
[40] T. Kristensen and R. Patel. Edge detection in a lateral inhibition network. In Proceedings of the 2002 International Joint Conference on Neural Networks. IJCNN'02 (Cat. No. 02CH37290), volume 2, pages 1620–1624, 2002. .
[41] D. Sagi, S. Hochstein, Lateral inhibition between spatially adjacent spatial-frequency channels?, Perception & Psychophysics 37 (1985) 315–322
[42] J.J. Letzkus, S.B.E. Wolff, A. Lüthi, Disinhibition, a circuit mechanism for associative learning and memory, Neuron 88 (2015) 264–276.
[43] P. Miller. An introductory course in computational neuroscience, chapter 6, pages 605–608. MIT Press, 2018. .
[44] R.A. Horn and C.R. Johnson. Topics in Matrix Analysis, volume 40, chapter 5, page 298. Cambridge University Press, 1991. .
[45] B. Cyganek, Object detection and recognition in digital images: theory and practice, chapter 2, John Wiley & Sons, 2013, pp. 152–153.
[46] R. Reams, Hadamard inverses, square roots and products of almost semidefinite matrices, Linear Algebra and its Applications 288 (1999) 35–43.
[47] C.F Van Loan. The ubiquitous kronecker product. Journal of computational and applied mathematics, 123: 85–100, 2000. .

Anastasia Giannari was born in Athens, Greece, in 1996. She received a Master of Engineering Degree in Biomedical Engineering from Imperial College London, London (UK) in 2018. In 2018, she joined the Control and Power Research Group at Imperial College London, London (UK) where she is currently working towards her Ph.D. degree in modelling and control of biomedical systems. Her research is mainly focused on modelling heterogeneous Hodgkin–Huxley neuronal networks with optimization methods.

Alessandro Astolfi was born in Rome, Italy, in 1967. He graduated in electrical engineering from the University of Rome in 1991. In 1992 he joined ETH-Zurich where he obtained a M.Sc. in information theory in 1995 and the Ph.D. degree with Medal of Honor in 1995 with a thesis on discontinuous stabilization of nonholonomic systems. In 1996 he was awarded a Ph.D. from the University of Rome La Sapienza for his work on nonlinear robust control. Since 1996 he has been with the Electrical and Electronic Engineering Department of Imperial College London, London (UK), where he is currently Professor of Nonlinear Control Theory and Head of the Control and Power Group. From 1998 to 2003 he was also an Associate Professor at the Department of Electronics and Information of the Politecnico of Milano. Since 2005 he has also been a Professor at Dipartimento di Ingegneria Civile e Ingegneria Informatica, University of Rome Tor Vergata. He has been/is Visiting Lecturer in Nonlinear Control in several universities, including ETHZurich (1995–1996); Terza University of Rome (1996); Rice University, Houston (1999); Kepler University, Linz (2000); SUPELEC, Paris (2001), Northeastern University (2013), University of Cyprus (2018-), Southeast University (2019-). His research interests are focused on mathematical control theory and control applications, with special emphasis for the problems of discontinuous stabilization, robust and adaptive control, observer design and model reduction. He is the author of more than 165 journal papers, of 30 book chapters and of over 380 papers in refereed conference proceedings. He is the author (with D. Karagiannis and R. Ortega) of the monograph "Nonlinear and Adaptive Control with Applications" (Springer-Verlag). He is the recipient of the IEEE CSS A. Ruberti Young Researcher Prize (2007), the IEEE RAS Googol Best New Application Paper Award (2009), the IEEE CSS George S. Axelby Outstanding Paper Award (2012), the Automatica Best Paper Award (2017). He is a "Distinguished Member" of the IEEE CSS, IEEE Fellow, IFAC Fellow, IET Fellow, and member of the Academia Europaea. He served as Associate Editor for Automatica, Systems and Control Letters, the IEEE Transactions on Automatic Control, the International Journal of Control, the European Journal of Control and the Journal of the Franklin Institute; as Area Editor for the International J. of Adaptive Control and Signal Processing; as Senior Editor for the IEEE Transactions on Automatic Control; and as Editor-inChief for the European Journal of Control. He is currently Editor-in-Chief of the IEEE Transactions on Automatic Control. He served as Chair of the IEEE CSS Conference Editorial Board (2010–2017) and in the IPC of several international conferences. He was/is a Member of the IEEE Fellow Committee (2016/2019–2022).